Supplementary data:

Impact of manganese on biofilm formation and cell morphology of *Candida parapsilosis* clinical isolates with different biofilm forming abilities

Sulman Shafeeq, Srisuda Pannanusorn, Youssef Elsharabasy, Bernardo Ramírez-Zavala, Joachim Morschhäuser and Ute Römling

Table S1: List of strains used in this study.

Strains/ Plasmids	Description	Source
C. parapsilosis		
ATCC 22019		Reference strain
SMI 416	Isolate from bloodstream infection	[1]
SMI 501	Isolate from bloodstream infection	[1]
SMI 630	Isolate from bloodstream infection	[1]
SMI 661	Isolate from bloodstream infection	[1]
SMI 681	Isolate from bloodstream infection	[1]
SMI 694	Isolate from bloodstream infection	[1]
SMI 706	Isolate from bloodstream infection	[1]
SMI 798	Isolate from bloodstream infection	[1]
SMI 828	Isolate from bloodstream infection	[1]
SMI 416 *bcr1*Δ	*BCR1* deletion in SMI 416	This study
ATCC 22019 *bcr1*Δ	*BCR1* deletion in ATCC 22019	This study
ATCC 22019 *bcr1*Δ + pBCR1	*BCR1* complementation in ATCC 22019 *bcr1*Δ strain	This study
Plasmids		
pBCR1CpM2	pSFS4 containing left and right flanking region of *BCR1* gene	[1]
pBCR1CpMK1	Left flanking region of *BCR1* in pBCR1CpM2 is replaced with *BCR1* gene including upstream region	[1]

References

1. Pannanusorn, S. *et al.* Characterization of biofilm formation and the role of BCR1 in clinical isolates of Candida parapsilosis. *Eukaryot. Cell* **13**, 438–451 (2014).

Figure S1: Impact of different concentrations of the divalent cations cobalt (Co^{2+}), copper (Cu^{2+}), iron (Fe^{3+}), nickel (Ni^{2+}) and zinc (Zn^{2+}) as nitrate salts on the biofilm forming ability of no (SMI 416), low (SMI 706) and high (SMI 828) biofilm formers of *C. parapsilosis* after 48 h at 37 °C (A, B and C) and 30 °C (D, E and F). Biofilms developed on a polystyrene surface in 96 well plates were stained with crystal violet and the OD_{600} was measured after dissolution in 30% acetic acid. Graphs represent the mean values calculated from three independent experiments with three biological replicates each. Error bars indicate the standard deviation.

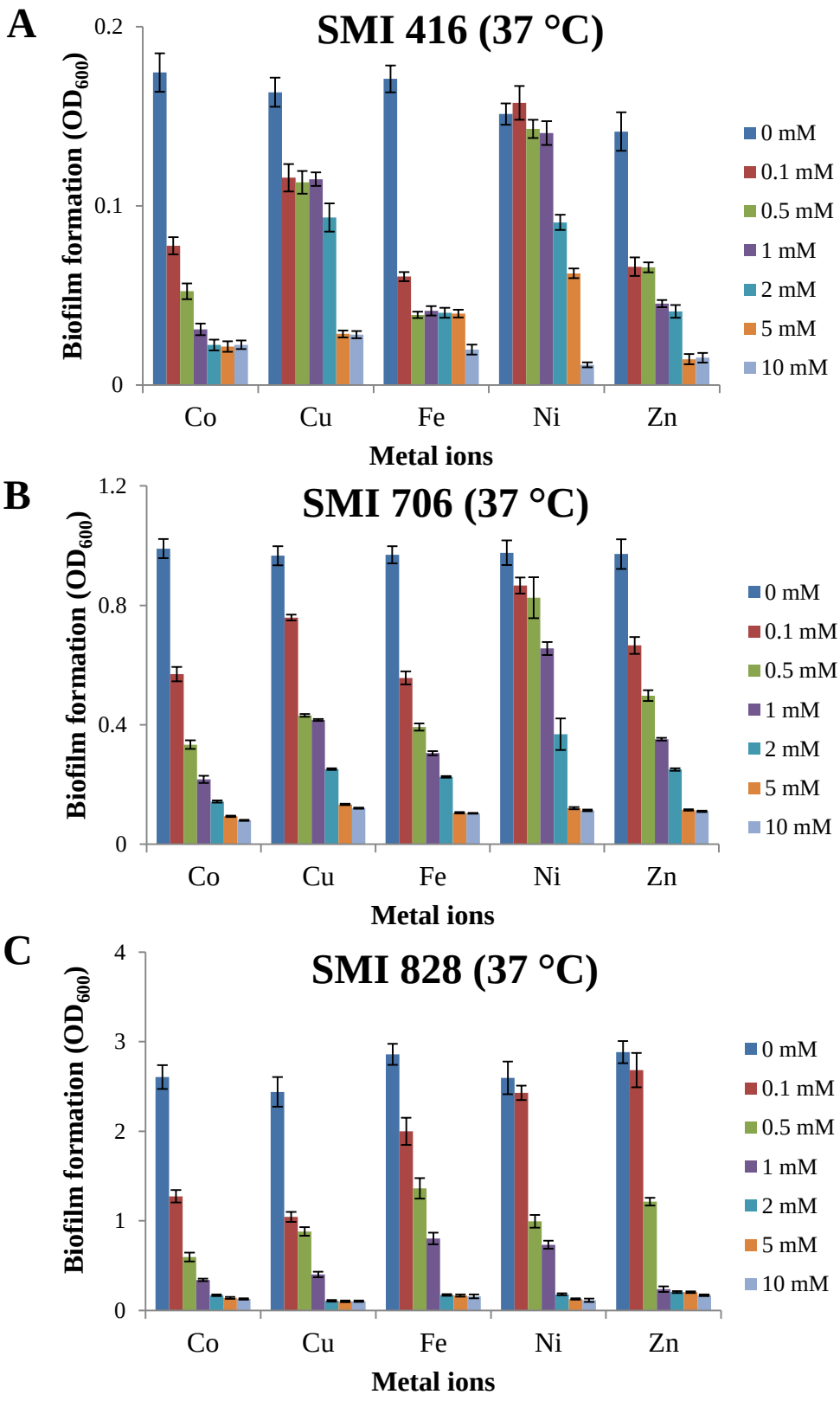

D

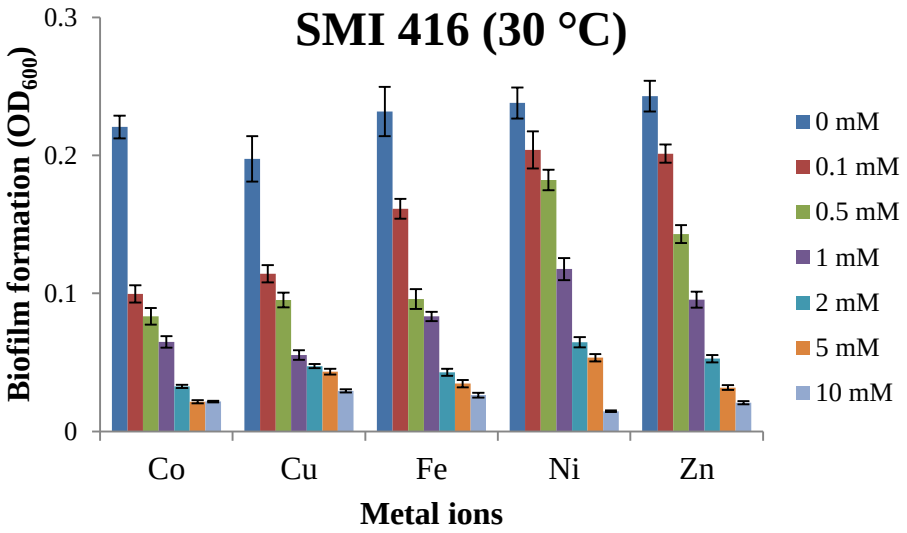
SMI 416 (30 °C)
Biofilm formation (OD600)
0.3
0.2
0.1
0
Co
Cu
Fe
Ni
Zn
Metal ions
0 mM
0.1 mM
0.5 mM
1 mM
2 mM
5 mM
10 mM

E

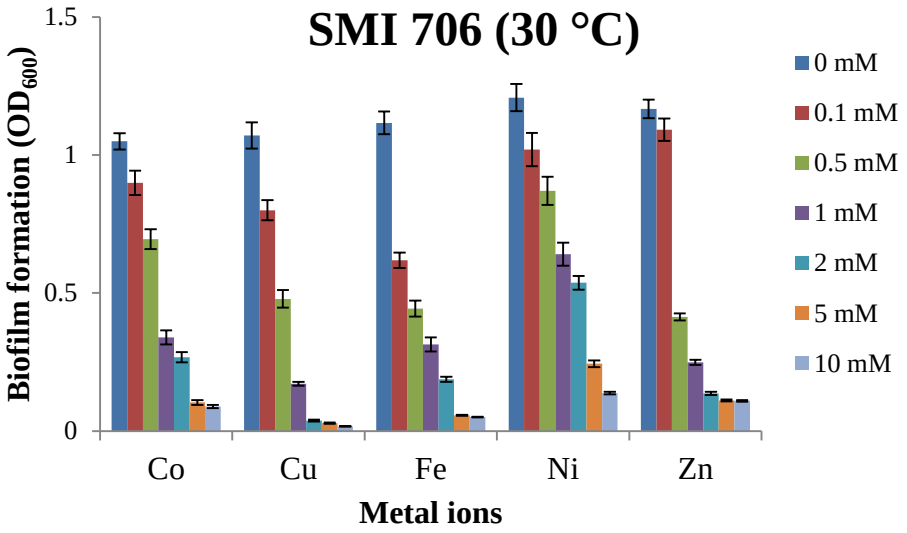
SMI 706 (30 °C)
Biofilm formation (OD600)
1.5
1
0.5
0
Co
Cu
Fe
Ni
Zn
Metal ions
0 mM
0.1 mM
0.5 mM
1 mM
2 mM
5 mM
10 mM

F

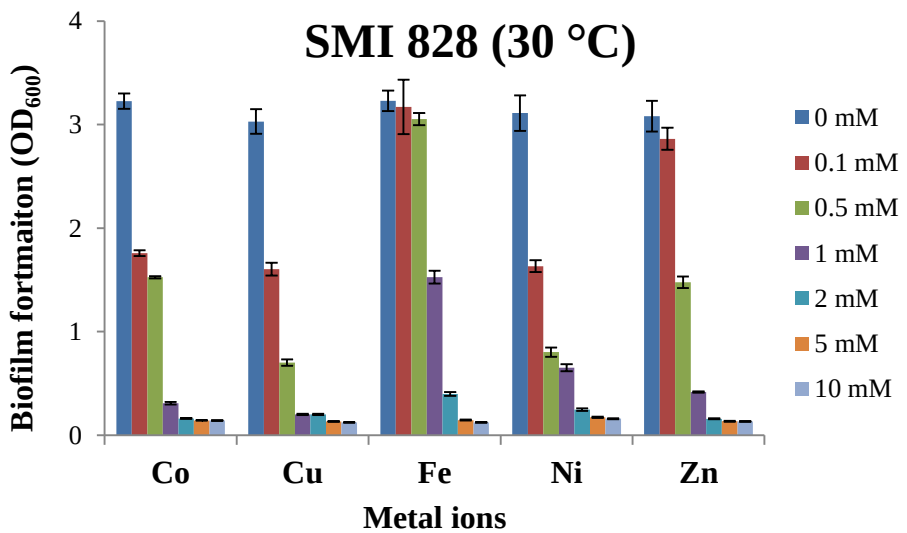
SMI 828 (30 °C)
Biofilm fortmaiton (OD600)
4
3
2
1
0
Co
Cu
Fe
Ni
Zn
Metal ions
0 mM
0.1 mM
0.5 mM
1 mM
2 mM
5 mM
10 mM

Figure S2: Impact of different concentrations of Mn^{2+} on biofilm forming ability of no (SMI 416 and ATCC 22019), low (SMI 706) and high (SMI 828) biofilm formers of *C. parapsilosis* at 37 °C after 48 h. Biofilms were developed on a polystyrene surface in 96 well plates were stained with crystal violet and the OD_{600} was measured after dissolution in 30% acetic acid. Graphs represent the mean values calculated from three independent experiments with biological replicates each and error bars indicate the standard deviation. Statistical significance of the differences in biofilm formation in the presence of Mn^{2+} compared to 0 mM Mn^{2+} was determined by one-way ANOVA (ns-not significant, *P < 0.05, **P < 0.01 and ***P < 0.001).

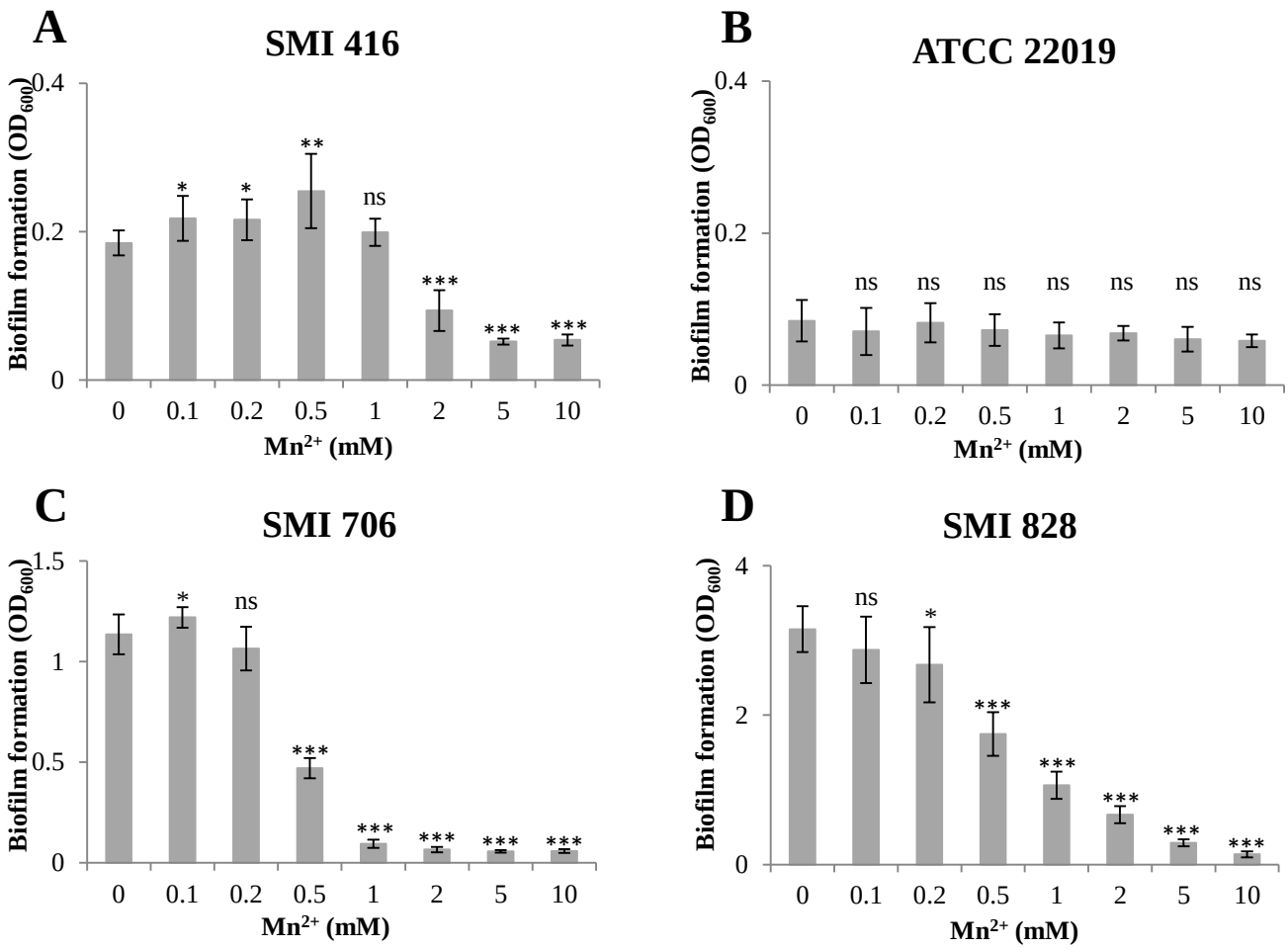

Figure S3: Impact of Mn^{2+} on the biofilm forming ability of *C. parapsilosis* ATCC 22019, SMI 501, SMI 630, SMI 661, SMI 681, SMI 694 and SMI 798 at 30 °C after 48 h. Biofilms were developed on a polystyrene surface in 96 well plates were stained with crystal violet and the OD_{600} was measured after dissolution in 30% acetic acid. Data points represent the mean values calculated from three independent experiments with three biological replicates each and error bars indicate the standard deviation.

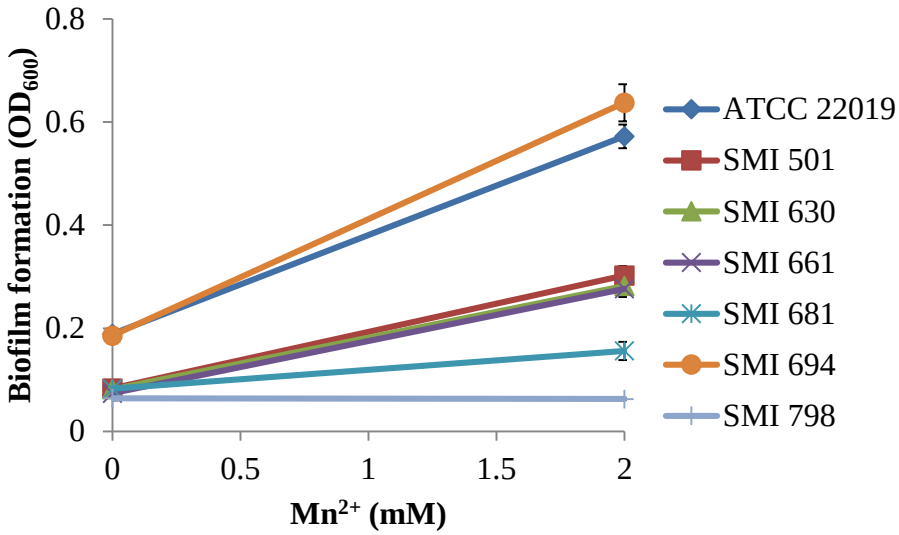

Figure S4: Impact of Mn^{2+} on the attachment of *C. parapsilosis* strains SMI 416 and ATCC22019, and their derivates. Attachment of wild type (SMI 416 and ATCC 22019), their *BCR1* mutants (SMI 416 *bcr1*Δ and ATCC 22019 *bcr1*Δ), and *BCR1* complementation (ATCC 22019 *bcr1*Δ+p*BCR1*) at 30 °C after 3 h of incubation (A and B). Relative attachment was calculated with attachment of the respective wild type at 0 mM Mn^{2+} set as 100%. Cells were allowed to attach to a polystyrene surface in 96 well plates and were subsequently stained with crystal violet. The OD_{600} was measured after dissolution of the crystal violet in 30% acetic acid. Graphs represent the mean values calculated from three independent experiments with three biological replicates each and error bars indicate the standard deviation. Statistical significance of the differences in attachment in the presence of 2 mM Mn^{2+} compared to 0 mM Mn^{2+} was calculated by one-way ANOVA (ns-not significant).

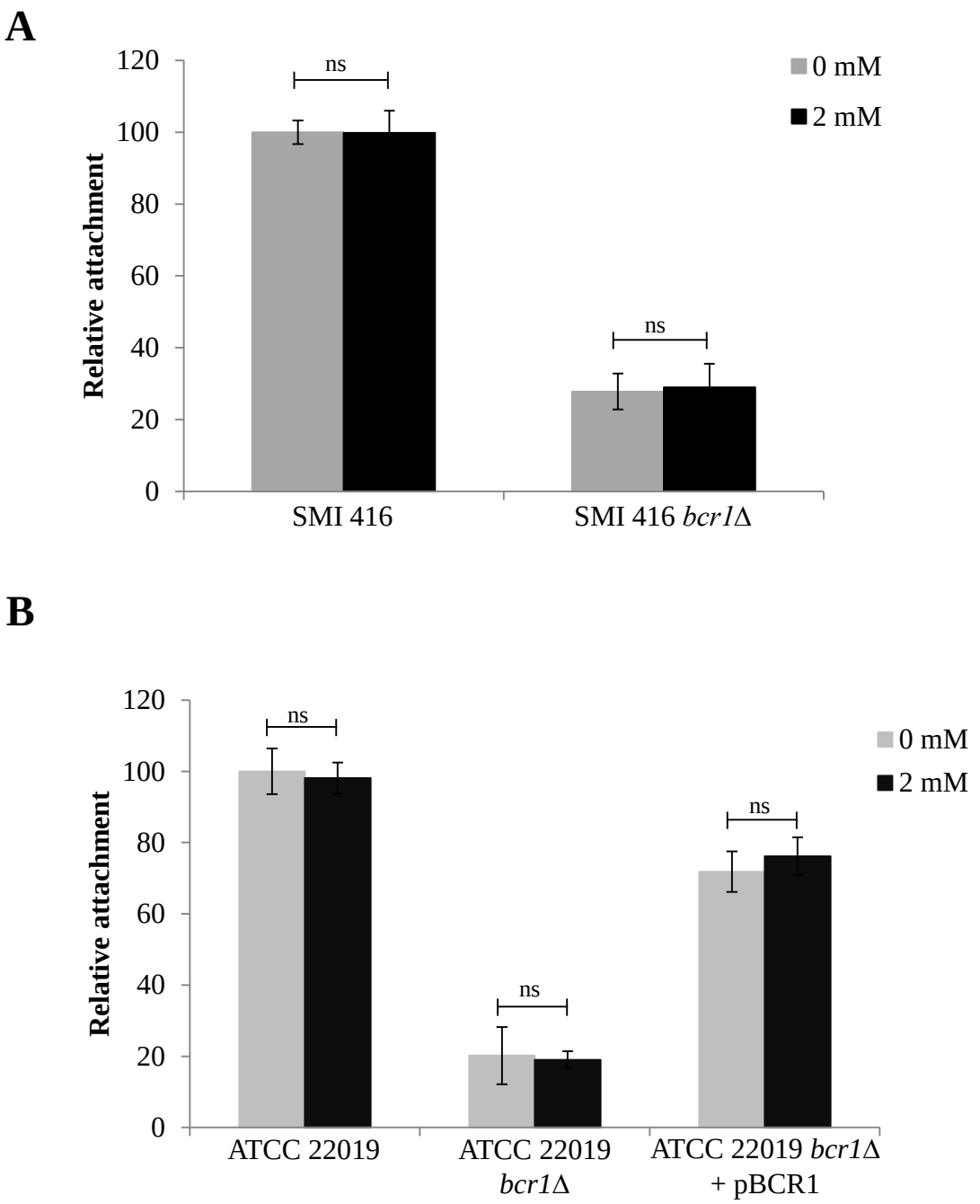

Figure S5: Cell viability in biofilms of *C. parapsilosis* SMI 416 wild type formed after 48 h at 30 ºC in the presence of 2 mM Mn^{2+}. (A) live cells; (B) dead cells; and (C) live/dead cells. Cells were stained with the LIVE/DEAD™ BacLight™ Viability Kit according to the manufacturer's instructions.

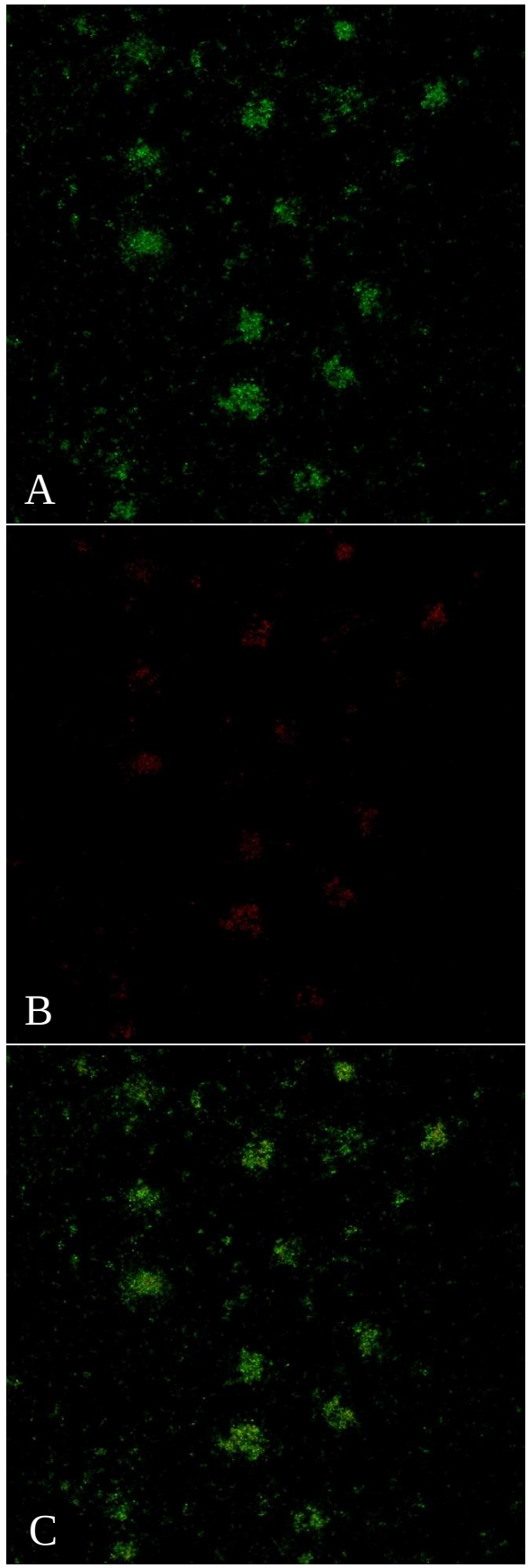

Figure S6: Impact of different concentrations of Mn^{2+} on the biofilm forming ability of wild type (SMI 416 and ATCC 22019), their *bcr1*Δ mutants (SMI 416 *bcr1*Δ and ATCC 22019 *bcr1*Δ) and *BCR1* complementation (ATCC 22019 *bcr1*Δ+p*BCR1*) at 37 ^{o}C (A and B). Biofilms developed on a polystyrene surface in 96 well plates were stained with crystal violet and the OD_{600} was measured after dissolution in 30% acetic acid. Graphs represent the mean values calculated from three independent experiments with three biological replicates each and error bars indicate the standard deviation. Statistical significance of the difference in biofilm formation (wild type SMI 416 and SMI 416 *bcr1*Δ) in the presence of Mn^{2+} compared to 0 mM Mn^{2+} was calculated by one-way ANOVA (ns-not significant, **P < 0.01, and ***P < 0.001).

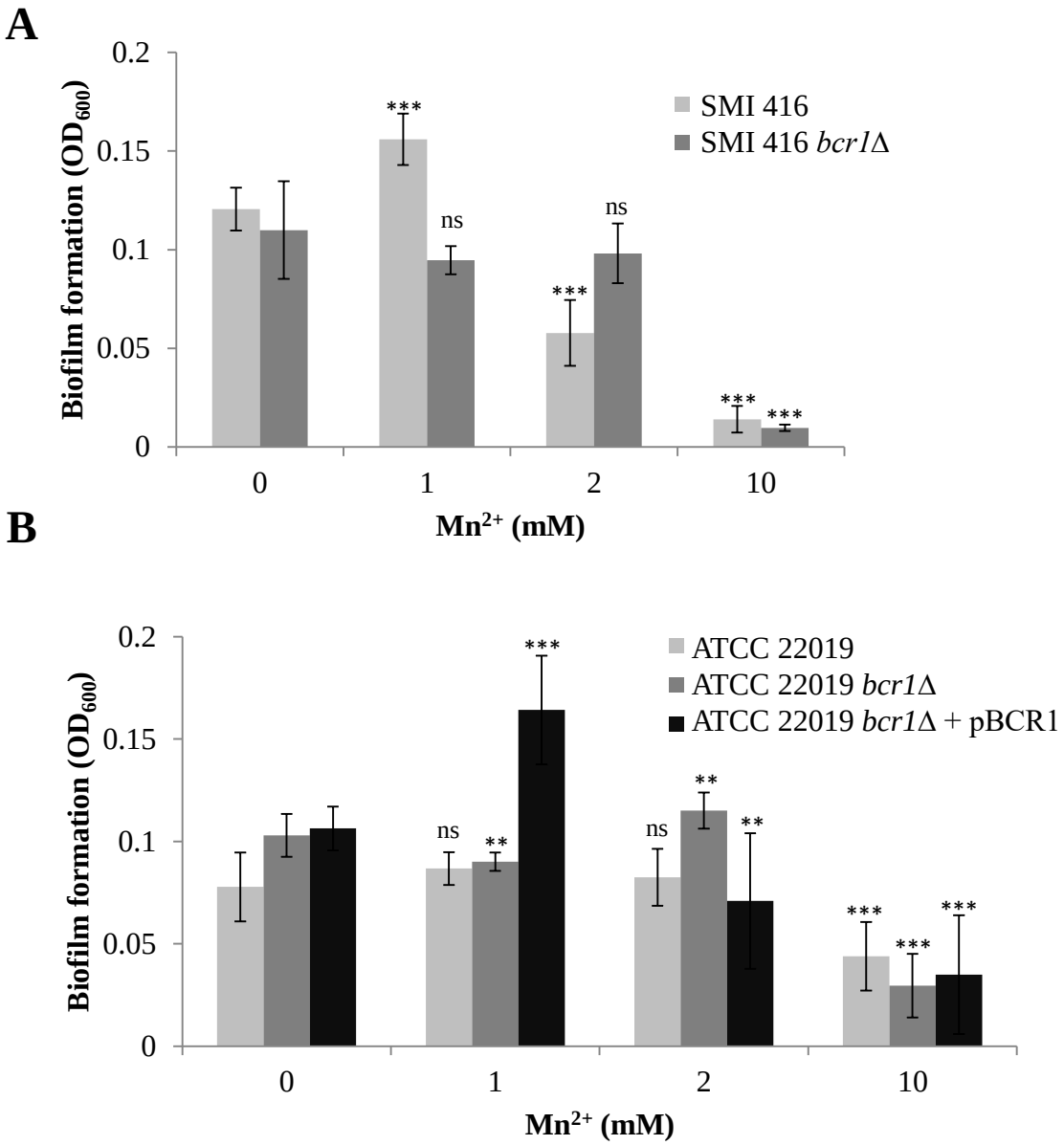

Figure S7: Pseudohyphae (A) and hyphae (B, C and D) stained with Calcofluor white (CFW).

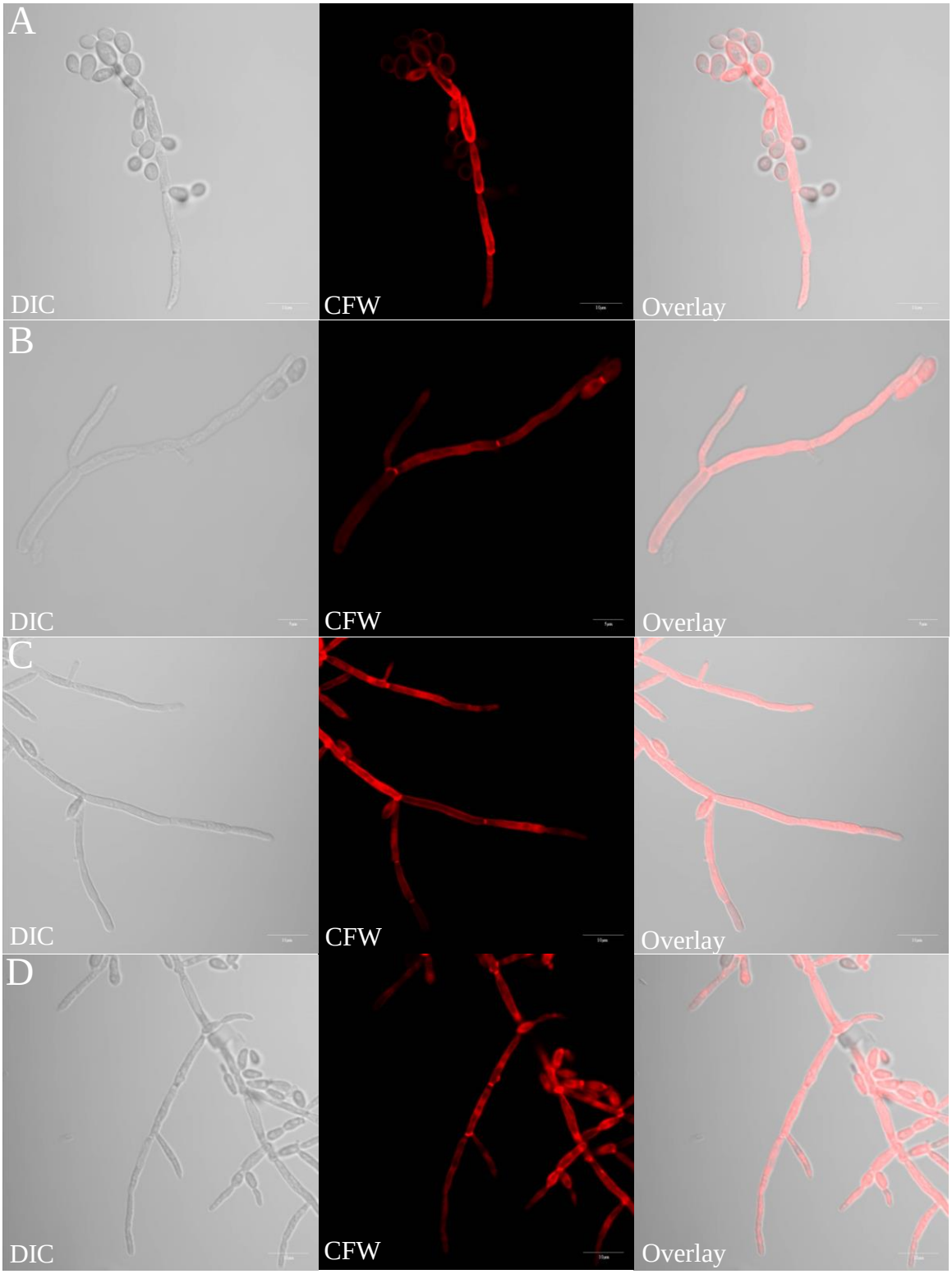

Figure S8: Multiple sequence alignment of Bcr1 of *C. viswanathii*, *C. tropicalis*, *C. dubliniensis*, *C. albicans*, *L. elongisporus*, *C. parapsilosis and C. orthopsilosis.*

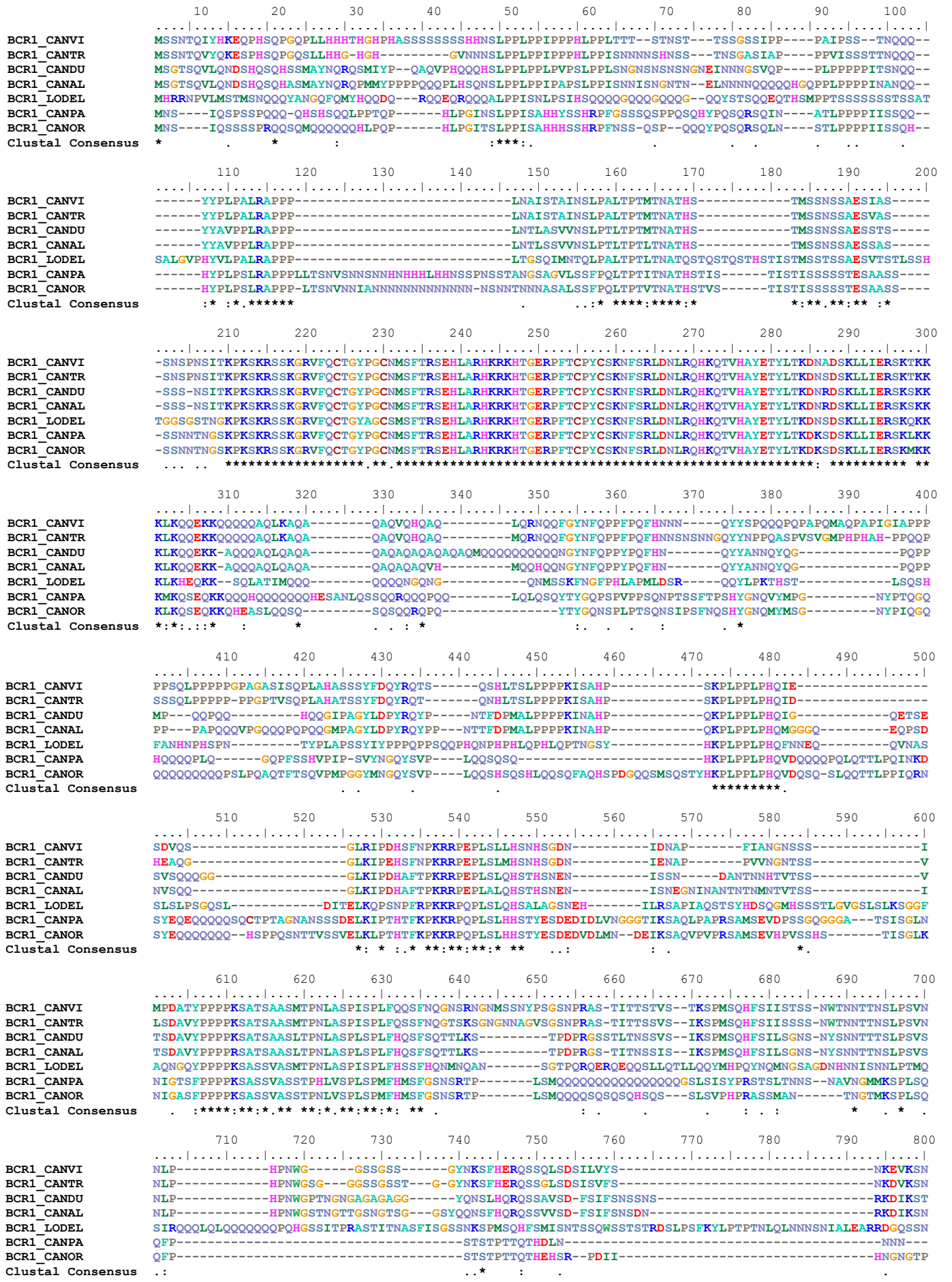

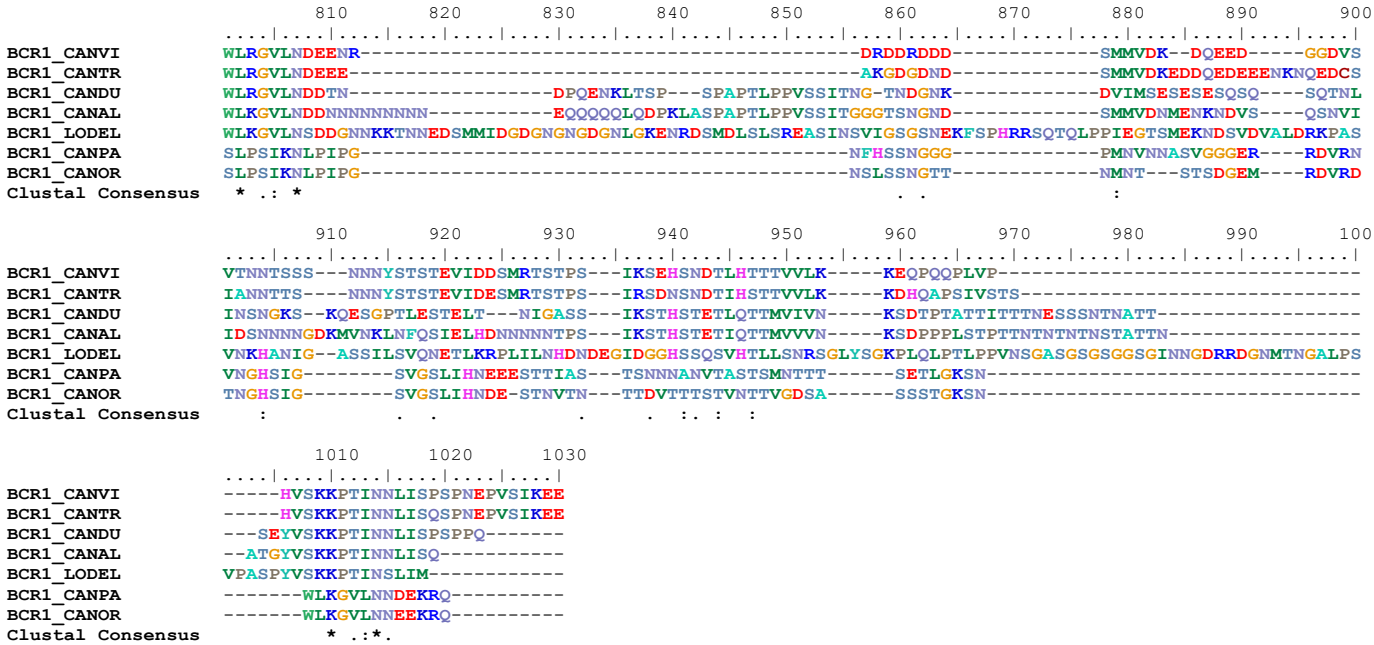
810 820 830 840 850 860 870 880 890 900
BCR1_CANVI WLRGVLNDEENR----------DRDDRDDD----------SMMVDK--DQEED-----GGDVS
BCR1_CANTR WLRGVLNDEEE----------AKGDGDND----------SMMVDKEDDQEDEEENKNQEDCS
BCR1_CANDU WLRGVLNDDTN----------DPQENKLTSP---SPAPTLPPVSSITNG-TNDGNK----------DVIMSESESESQSQ----SQTNL
BCR1_CANAL WLKGVLNDDNNNNNNNNN----------EQQQQQLQDPKLASPAPTLPPVSSITGGGTSNGND----------SMMVDNMENKNDVS----QSNVI
BCR1_LODEL WLKGVLNSDDGNNKKTNNEDSMMIDGDGNGNGDGNLGKENRDSMDLSLSREASINSVIGSGSNEKFSPHRRSQTQLPPIEGTSMEKNDSVDVALDRKPAS
BCR1_CANPA SLPSIKNLPIPG----------NFHSSNGGG----------PMNVNNASVGGGER----RDVRN
BCR1_CANOR SLPSIKNLPIPG----------NSLSSNGTT----------NMNT---STSDGEM----RDVRD
Clustal Consensus
910 920 930 940 950 960 970 980 990 1000
BCR1_CANVI VTNNTSSS---NNNYSTSTEVIDDSMRTSTPS---IKSEHSNDTLHTTTVVLK-----KEQPQQPLVP----------
BCR1_CANTR IANNTTS----NNNYSTSTEVIDESMRTSTPS---IRSDNSNDTIHSTTVVLK-----KDHQAPSIVSTS----------
BCR1_CANDU INSNGKS--KQESGPTLESTELT---NIGASS---IKSTHSTETLQTTMVIVN-----KSDTPTATTITTTNESSSNTNATT----------
BCR1_CANAL IDSNNNNGDKMVNKLNFQSIELHDNNNNNTPS---IKSTHSTETIQTTMVVVN-----KSDPPPLSTPTTNTNTNTNSTATTN----------
BCR1_LODEL VNKHANIG--ASSILSVQNETLKRPLILNHDNDEGIDGGHSSQSVHTLLSNRSGLYSGKPLQLPTLPPVNSGASGSGSGGSGINNGDRRDGNMTNGALPS
BCR1_CANPA VNGHSIG--------SVGSLIHNEEESTTIAS---TSNNNANVTASTSMNTTT------SETLGKSN----------
BCR1_CANOR TNGHSIG--------SVGSLIHNDE-STNVTN---TTDVTTTSTVNTTVGDSA------SSSTGKSN----------
Clustal Consensus
1010 1020 1030
BCR1_CANVI -----HVSKKPTINNLISPSPNEPVSIKEE
BCR1_CANTR -----HVSKKPTINNLISQSPNEPVSIKEE
BCR1_CANDU ---SEYVSKKPTINNLISPSPPQ-------
BCR1_CANAL --ATGYVSKKPTINNLISQ----------
BCR1_LODEL VPASPYVSKKPTINSLIM----------
BCR1_CANPA -------WLKGVLNNDEKRQ----------
BCR1_CANOR -------WLKGVLNNEEKRQ----------
Clustal Consensus